Chemical Science

ROYAL SOCIETY OF CHEMISTRY

EDGE ARTICLE

View Article Online
View Journal | View Issue

Cite this: *Chem. Sci.*, 2024, **15**, 18601

All publication charges for this article have been paid for by the Royal Society of Chemistry

Received 21st August 2024
Accepted 4th October 2024

DOI: 10.1039/d4sc05625f

rsc.li/chemical-science

Highly efficient pure organic near-ultraviolet (NUV) electro-fluorescent materials with high electron mobility and improved hole mobility†

Huayi Zhou,[a] Runze Wang,[a] Mizhen Sun,[a] Yannan Zhou,[a] Li Zhang,[a] Jingru Song,[a] Qikun Sun,[a] Shi-Tong Zhang,*[b] Wenjun Yang [a] and Shanfeng Xue *[a]

The lack of blue-emissive materials with high efficiency and excellent color purity commonly represents a pivotal obstacle in the development of organic light-emitting diodes (OLEDs). In this work, two blue to near-ultraviolet (NUV) donor–π–acceptor (D–π–A) emitters based on a fluorene π-bridge, **9-PCZCFTZ** and **3-PCZCFTZ**, are thus designed and synthesized, and non-doped devices derived from these two materials exhibit electroluminescence (EL) emission peaks at 404 nm and 417 nm, respectively. Interestingly, due to the specific stacking, a phenomenon appears in both materials in which the mobility of the electron is much higher than that of the hole, prompting us to use host doping to increase the hole mobilities, which ultimately leads to excellent OLED performances. As a result, the maximum external quantum efficiency (EQE_{max}) values of **9-PCZCFTZ** and **3-PCZCFTZ** in the doped devices reach as high as 14.5% and 10.8% respectively. Notably, both OLEDs show high blue purity very close to the BT.2020 standard.

Introduction

In recent decades, organic light-emitting diodes (OLEDs) have attracted increasing attention in the field of flat panel displays due to their excellent performance and low cost.[1–5] Commonly, the emitter layer is regarded as a crucial part that restricts the development of OLEDs; thus, outstanding OLED performances are determined by the parameters of blue to near-ultraviolet (NUV) materials, which can be seen as important indicators. However, there are still few reports[6,7] of high-efficiency blue-to-NUV materials with a CIE coordinate (y) of less than 0.10 that conform to the standard blue CIE coordinates of (0.131, 0.046) set by International Telecommunication Union-Radiocommunication (ITU-R) Sector Recommendation BT.2020 for Ultra High Definition Television (UHDTV).[8–12] Rationally adjusting the excited state of materials is a very effective way to obtain highly efficient emitters with high color purity. It is well known that electrons and holes are bound together by electrostatic Coulomb forces to form localization (LE) state excitons or charge-transfer (CT) state excitons. The LE state exhibits strong confinement of the electron cloud, which promotes radiative transitions of photons to the ground state for luminescence. As a result, molecules in the LE state typically possess high PLQY and short-wavelength emission. However, molecules with purely LE excited states are usually not conducive to the transfer of triplet excitons to the singlet state for utilization, making it difficult to achieve high exciton utilization efficiency (EUE).[13–15] The charge-transfer (CT) excited state with weak binding energy has proved to be of great significance in enhancing the EUE, which is well known for thermally activated delayed fluorescence (TADF) materials and their OLEDs.[16–20] However, there is a fatal drawback to the CT excited state, that is, the very small transition orbit overlaps severely restrict its radiative transition, resulting in poor PLQY. In light of this, the hybridized local and charge transfer (HLCT) excited state has proved to be a fruitful solution to the tradeoff between the simultaneous realization of high EUE and PLQY. The HLCT excited state contains hybridized LE and CT excited components, among which the LE component guarantees high luminescence efficiency and color purity, and the CT component is responsible for high EUE.[10,21–25] However, the molecular design of CT materials and early HLCT materials has commonly consisted of a directly bonded donor and acceptor,[26] which can easily form a twisted intermolecular charge-transfer (TICT) state resulting in relatively lower exciton energy with a wide photoluminescence (PL) spectrum. Therefore, in order to obtain highly efficient blue-to-NUV fluorescent materials and fluorescent OLEDs, further rational molecular design is needed.

In addition to high PLQY, high EUE and color purity, another important issue that should be considered is carrier transportation (including hole and electron mobilities: μ_{hole} and μ_{elec}, respectively). Recently, we found that a donor–π–acceptor

[a]*Key Laboratory of Rubber-Plastics of the Ministry of Education, School of Polymer Science & Engineering, Qingdao University of Science and Technology, Qingdao 266042, P. R. China. E-mail: sfxue@qust.edu.cn*

[b]*State Key Laboratory of Supramolecular Structure and Materials, Institute of Theoretical Chemistry, College of Chemistry, Jilin University, Changchun 130012, P. R. China. E-mail: stzhang@jlu.edu.cn*

† Electronic supplementary information (ESI) available. CCDC 2176493 and 2176856. For ESI and crystallographic data in CIF or other electronic format see DOI: https://doi.org/10.1039/d4sc05625f

(D–π–A) structure with fluorene as a π-bridge can be an effective solution to the above demands for highly efficient blue-emissive materials and OLEDs.[27] A high EQE of 9.8% with fast and balanced carrier mobilities of $\mu_{hole} = 5.6 \times 10^{-5}$ cm^2 V^{-1} s^{-1} and $\mu_{elec} = 6.6 \times 10^{-5}$ cm^2 V^{-1} s^{-1}, respectively, were achieved in this work. In addition, optimizing the device structure to achieve balanced carrier mobility represents an effective strategy for further enhancing the efficiency of OLED devices. It is well known that the electron mobility of organic materials tends to be much lower than that of holes,[28] making the device design process highly demanding for the electron transporting functional layer and rendering device design difficult. Further work on the regulation of the electron mobility achieved a μ_{elec} of 3.57×10^{-4} cm^2 V^{-1} s^{-1} and an enhanced EQE of 11.1%.[29] These data belong to the group of best results compared to previous works on blue-emissive HLCT OLEDs, yet their light color is still far from the demands for high-definition displays. Therefore, further structural optimization efforts for molecules and devices are needed to realize deep-blue or NUV emissive materials with high OLED performance.

In this work, a new strategy to ameliorate the unbalanced mobility using a doped device is carried out and found to significantly promote the performance of blue materials. *N*-Phenylcarbazole with different bonding positions was selected as the donor (D), and triazole was utilized as the acceptor (A) to construct novel D–A molecules. In detail, the D and A moieties are linked indirectly by a fluorene bridge to construct the corresponding asymmetric D–π–A type molecules **9-PCZCFTZ** and **3-PCZCFTZ** (Scheme 1). Carbazole is generally seen as a weak or moderately electron-donating unit with unique geometric and electronic structures; carbazole units have been used as building blocks for improving hole injection and transport properties.[30–33] Triazole is regarded as an electron-accepting unit and is widely used as a building block to construct electron-transporting materials for OLEDs.[34–36] Notably, the fluorene structure has demonstrated dual functions, both enhancing hole mobility and effectively regulating face-to-face molecular stacking; it has even been claimed to play an important role in molecular stacking. As a result, both molecules exhibit bright blue-to-NUV emission with electroluminescence (EL) emission peaks locating at 404 nm and 417 nm respectively. Additionally, theoretical calculations indicate that the construction of an HLCT state under suitable torsion in a D–π–A structure enables high efficiency to be achieved. The EQE values of both molecules are around 5%, which represents one of the best recorded results among non-doped UV OLEDs. Furthermore, the μ_{elec} values of the two molecules are 1.11×10^{-5} and 2.33×10^{-5} cm^2 V^{-1} s^{-1}, respectively, which are both superior to their μ_{hole} values. Then, two doped devices were fabricated in order to achieve a balance between carrier injection/transport, and excellent results were obtained as expected. Significantly, the EQE of **9-PCZCFTZ** increased to 14.5% with a CIE coordinate of (0.163, 0.045), which contributes to overcoming the aforementioned obstacles, *i.e.*, the urgent need for improvement in efficiency and color purity; moreover, these achievements prove that it is undoubtably feasible to achieve balanced carrier mobilities by doping a hole-type host as an efficient strategy.

Results and discussion

Synthesis and molecular design

As mentioned above, carbazole derivatives are utilized as electron donors and triazoles are used as electron acceptors. Generally, triazoles exhibit excellent electron accepting ability, while benzene rings around the triazole give the molecule a certain degree of distortion in order to avoid serious quenching phenomena. As specific advantages, the high energy of triazoles is also beneficial for the molecules to show blue emission, and variation of the connection site in carbazole can simultaneously alter the molecular distortion and regulate the stacking of molecules, ultimately tuning the carrier transport properties of the targeted molecules. The synthetic strategy and data for **9-PCZCFTZ** and **3-PCZCFTZ** are illustrated in Scheme 1 and Fig. S1–S7.† Here, the alkyl group is bonded by fluorene under the action of tetrabutylammonium bromide, while connections between the phenyl-carbazole (PCZ), the fluorene bridge and the triazoles (TZ) are simply achieved *via* a Suzuki coupling reaction. The chemical structure was characterized using NMR and high-resolution mass spectrometry (MS).

Theoretical calculations

To obtain a deeper understanding of the electronic structures of two investigated molecules, their optimized molecular structures and the spatial distributions of their HOMOs and LUMOs were calculated using density functional theory (DFT) and time-dependent DFT (TDDFT). As illustrated in Fig. 1a, the twisting angles of the two molecules are all relatively small, with the exception of the larger angle between 4-benzene and the triazole

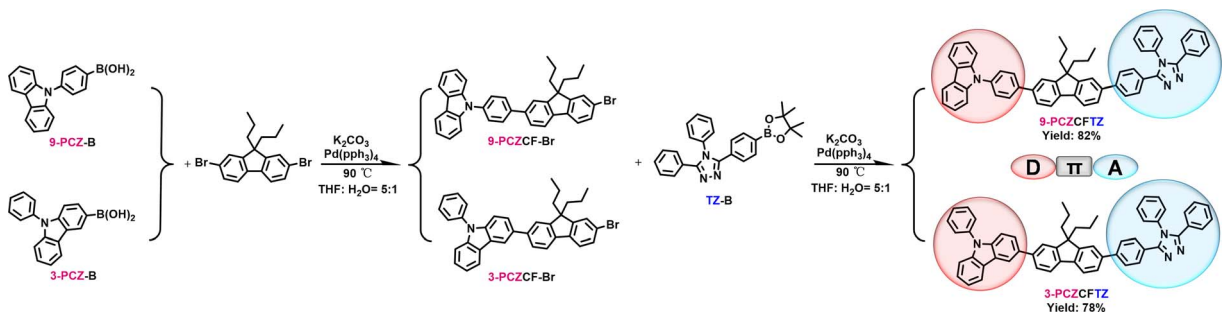

Scheme 1 Molecular design and synthesis routes of **9-PCZCFTZ** and **3-PCZCFTZ**.

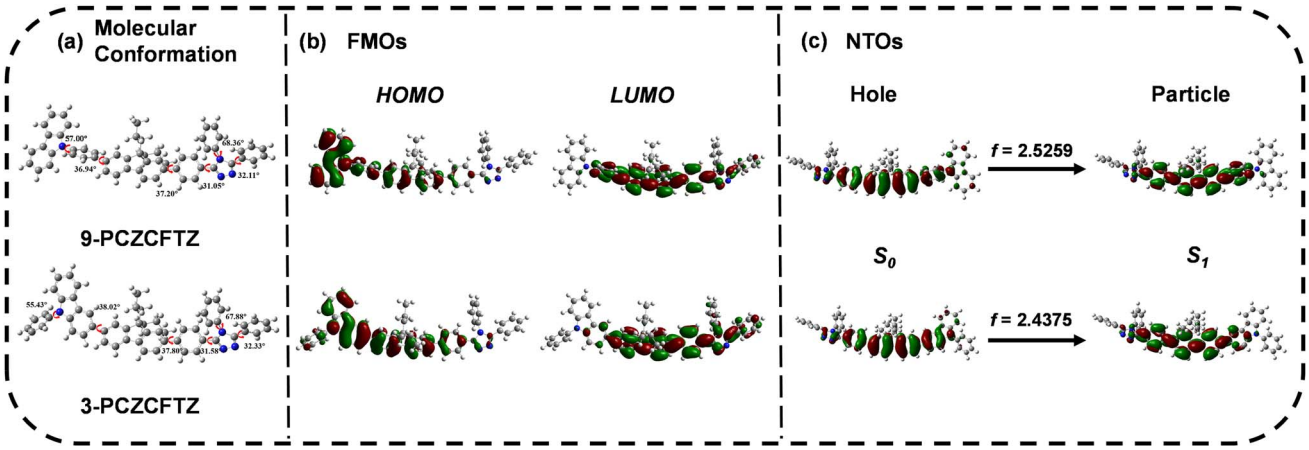

Fig. 1 (a) Geometries and structural formulas, (b) frontier orbital distributions, and (c) the $S_0 \rightarrow S_1$ natural transition orbits (NTOs) of the two investigated molecules.

(68.36° for **9-PCZCFTZ**, 67.88° for **3-PCZCFTZ**), implying that both of them exhibit effective π-conjugation, which benefits the formation of large excited state oscillator strength and high photoluminescent quantum yield (PLQY) values. Large overlaps of electron clouds also existed in the $S_0 \rightarrow S_1$ natural transition orbits (NTOs) of the two materials, corresponding to their high oscillator strengths. As shown in Fig. 1b, the highest occupied molecular orbitals (HOMOs) of the two molecules are both distributed on the donor and the fluorene bridge and, similarly, their lowest unoccupied molecular orbitals (LUMOs) are distributed on the fluorene bridge and the triazole unit. The electron clouds of the HOMO and LUMO orbitals overlap on the fluorene bridge in both compounds, and the frontier molecular orbitals (FMOs) of the molecules exhibit characteristics of both overlap and separation. These are typical features of the HLCT mechanism, which are beneficial to realize high exciton utilization and efficiency in practical devices. Furthermore, **9-PCZCFTZ** shows a larger overlap than **3-PCZCFTZ**, providing a smaller dipole moment.

Thermal stabilities and electrochemical properties

In order to explore the feasibility of utilizing the target molecules for OLED fabrication, the thermal properties of **9-PCZCFTZ** and **3-PCZCFTZ** were characterized. As shown in Fig. S9 and Table S1,† the melting temperature (T_m) was found to be 293 °C for **9-PCZCFTZ**, while the glass-transition temperature (T_g) of **3-PCZCFTZ** seems to be above 130 °C; the decomposition temperatures (T_d) of the two materials are both above 450 °C, proving that it enables the formation of dense films for the materials as organic light emitting layers in OLEDs without diminishment of their properties under the high temperatures of evaporation. The electrochemical properties of the compounds were determined through cyclic voltammetry (Fig. S10†), and subsequently, the HOMO and LUMO energy levels of both compounds were calculated based on their oxidation and reduction potentials. Specifically, **9-PCZCFTZ** exhibited a HOMO of −5.40 eV and a LUMO of −2.31 eV, while **3-PCZCFTZ** displayed a HOMO of −5.31 eV and a LUMO of −2.31 eV. **9-PCZCFTZ** demonstrated a slightly wider electrochemical bandgap (E_g = 3.09 eV) compared to that observed for **3-PCZCFTZ** (E_g = 3.00 eV), which will result in bluer emission for **9-PCZCFTZ**.

Photophysical properties

The absorption and PL spectra of the two investigated molecules are illustrated in Fig. 2 in two distinct states; one is at a concentration of 10^{-5} M in THF solution, and the other is in the film state. The corresponding parameters are listed in Table 1. Both the molecules show similar π–π* main absorption peaks, with gradual red-shifts corresponding to their molecular π-conjugated skeleton and reduction of the HOMO–LUMO energy gaps. The absorption and PL spectra of the two molecules thus show totally consistent red-shift trends. As an example, the PL peaks are located at 427 nm and 444 nm for **9-PCZCFTZ** and **3-PCZCFTZ** in the film state, respectively. However, the intramolecular charge transfer (ICT) characteristic of **3-PCZCFTZ** is stronger than that of **9-PCZCFTZ** due to its enhanced degree of conjugation.

The solvatochromic effects of the two molecules also correspond to their ascending CT characteristics. The red-shifts of **9-PCZCFTZ** and **3-PCZCFTZ** are around 25 nm and 44 nm, respectively (Fig. 2c), and varied with the distinct solvent polarities from *n*-hexane to acetonitrile. We further estimated the dipole moments of the excited state (μ_e) following the Lippert–Mataga model, in which small dipole moments (μ_e = 6–7 D for pure LE-state molecules) can be found in low-polarity solvents, and oppositely, the dipole moments show great enhancements in high-polarity solvents (μ_e = 23 D for pure CT-state molecules). The two-section linear relations (Fig. 2d) indicate the co-existence of LE and CT in both molecules; additionally, combining these results with those obtained from the single-exponential fluorescence decay (Fig. S8†), it can also be concluded that the molecules exhibit typical HLCT characteristics.

Carrier mobilities and single crystal structures

Initially, we fabricated hole-only and electron-only separated devices using the two materials to estimate their carrier

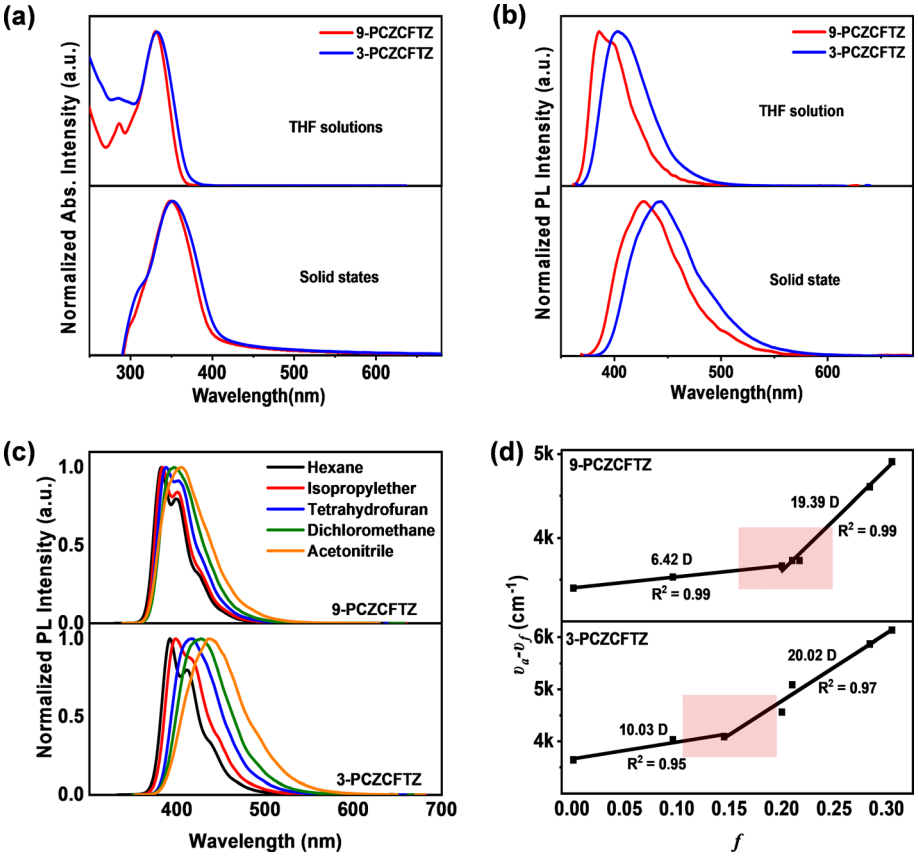

Fig. 2 (a) Normalized UV-vis spectra in THF solution (10^{-5} M) and neat film. (b) Normalized PL spectra in THF solution (10^{-5} M) and neat film. (c) Normalized PL spectra in different solvents with increasing polarity and (d) linear correlation of the orientation polarization (*f*) of the solvent media with the Stokes shift (ν_a–ν_f) for the two molecules.

mobilities (μ_{hole} and μ_{elec}) (Fig. 3 and Table S1†). Indeed, the two molecules show similar μ_{elec} values, 1.11×10^{-5} cm^2 V^{-1} s^{-1} for **9-PCZCFTZ** and 2.33×10^{-5} cm^2 V^{-1} s^{-1} for **3-PCZCFTZ**, which are more than an order of magnitude higher than their μ_{hole} values, which are 1.07×10^{-6} and 5.49×10^{-7} cm^2 V^{-1} s^{-1} for **9-PCZCFTZ** and **3-PCZCFTZ**, respectively, indicating that **9-PCZCFTZ** has higher hole mobility and a more balanced carrier mobility than **3-PCZCFTZ**. Since π-stacking intermolecular aggregation may cause significant impacts on the device performance, their single-crystal structures were prepared in order to explore the correlation between the mobility and stacking mode. As shown in Fig. 4 (single crystal data are listed in Table S2†), the single-crystal structures of **9-PCZCFTZ** and **3-PCZCFTZ** exhibit similar stacking patterns: PCZ stacks in a face-to-face configuration, as does TZ, indicating that the electron and hole providers with similar ability will compete with each other. Moreover, abundant C–H···π interactions occurred in the two molecules, which are beneficial for constructing different hole or electron transport channels. Interestingly, for **9-PCZCFTZ**, the "donor–donor" interactions between two adjacent molecules were more abundant than in **3-PCZCFTZ**, providing a closer intermolecular interaction between the "donor–donor" and "acceptor–acceptor" combinations. This result provides a convincing explanation for the fact that **9-PCZCFTZ** shows higher and more balanced carrier mobilities.

Electroluminescence performances

In order to survey the electroluminescence properties, non-doped OLEDs based on two materials were further fabricated

Table 1 Photophysical properties of the two molecules

	λ_{PL}[a] [nm]					Φ_{PL}[b] [%]		τ[c] [ns]	
Molecules	Hexane	THF	DCM	Acetonitrile	Film	THF	Film	THF	Film
9-PCZCFTZ	387	392	401	411	427	1.00	0.46	0.83	1.96
3-PCZCFTZ	392	417	428	436	444	0.99	0.60	0.98	2.81

[a] λ_{PL}: maximum emission wavelength, concentration: 10^{-5} M. [b] Φ_{PL}: absolute fluorescence quantum efficiency. [c] τ: fluorescence lifetime.

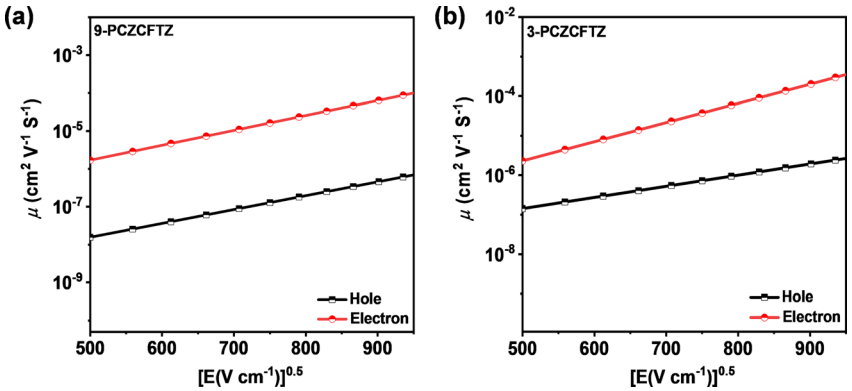

Fig. 3 Estimated hole and electron mobilities of the two materials under different electric fields. Configuration of the hole-only device: ITO/HATCN (20 nm)/EML (80 nm)/HATCN (20 nm)/Al (100 nm). Configuration of the electron-only device: ITO/LiF (1 nm)/TPBi (10 nm)/EML (80 nm)/LiF (1 nm)/Al (100 nm).

with a typical device structure of ITO/PEDOT:PSS (40 nm)/TCTA (20 nm)/emissive materials (20 nm)/TPBi (30 nm)/LiF (1 nm)/Al (100 nm) (where the emissive material was **9-PCZCFTZ** in N1 and **3-PCZCFTZ** in N2), which were characterized using their cyclic-voltammetry (CV) curves and HOMO/LUMO energy levels (Fig. S10†). As shown in Fig. 5 and Table 2, the two molecules **9-PCZCFTZ** and **3-PCZCFTZ** both exhibit bright NUV light (404 nm and 417 nm), and their EQE_{max} values are around 5% with CIE coordinates of (0.160, 0.100) and (0.158, 0.135), respectively, which seem to be ordinary efficiencies in the deep blue to NUV range. The OLED performances indicate that no significant difference was detected in the EQE values in the non-doped devices, as the value of **9-PCZCFTZ** is only slightly higher than that of **3-PCZCFTZ**, revealing that promoting the balance between μ_{hole} and μ_{elec} represents an effective way to improve EQE, especially in the case of **3-PCZCFTZ**.

Doped OLEDs based on the two materials were then fabricated with a device structure of ITO/PEDOT:PSS (40 nm)/NPB (80 nm)/TCTA (20 nm)/emissive materials (20 nm)/TPBi (35 nm)/LiF (1 nm)/Al (100 nm) (where the emissive material was 1 wt% **9-PCZCFTZ** : CBP in D1 and 1 wt% **3-PCZCFTZ** : CBP in D2), in which CBP was a hole-type host material to suppress the molecular aggregation and improve the μ_{hole} values. As shown in Table 2 and Fig. S11,† the doped devices exhibit much better device performance with EQE_{max} values of 14.5% and 10.8% for **9-PCZCFTZ** and **3-PCZCFTZ**, respectively, which were almost 2 to 4 times those of their non-doped devices. Impressively, the emission peaks of the doped devices were located at 390 nm and 398 nm with CIE coordinates of (0.163, 0.045) and (0.159, 0.051), respectively; their performances were greatly improved, benefiting from the fact that these two materials more easily extract energy from the host materials in the doped device; moreover, the physical dispersion leads to rearrangement on them. Hence, **9-PCZCFTZ** obtains a larger advantage, which can be rapidly expanded, and higher device efficiency can be further obtained as expected. In addition, the deep hole-transmission

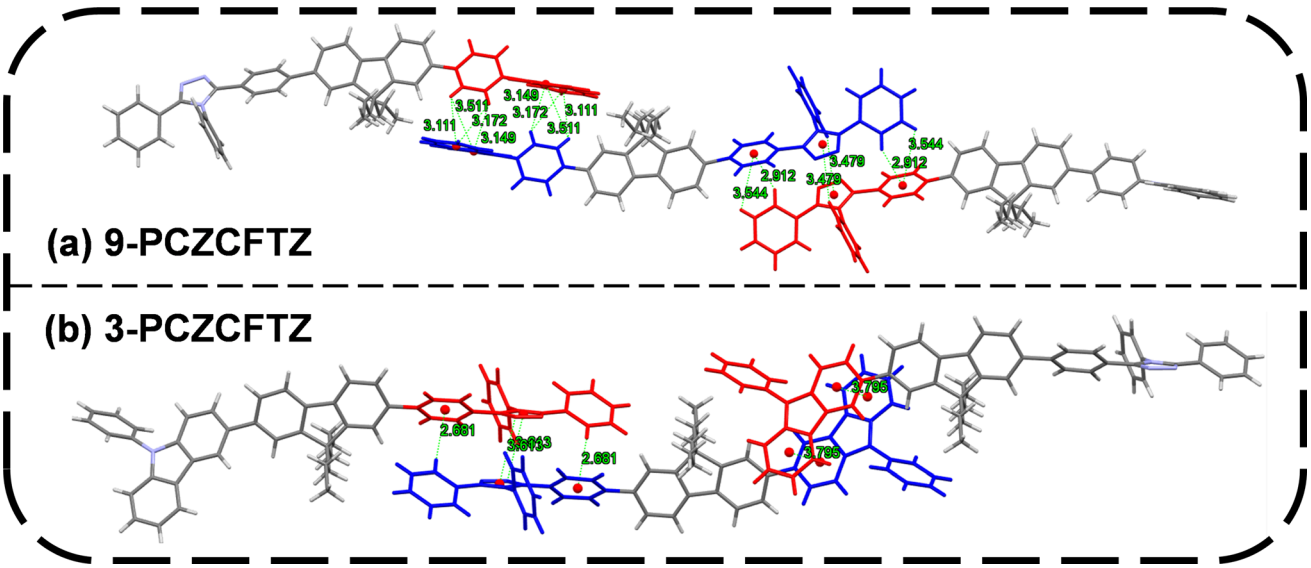

Fig. 4 Molecular stacking patterns and corresponding schematic diagrams of (a) 9-PCZCFTZ and (b) 3-PCZCFTZ.

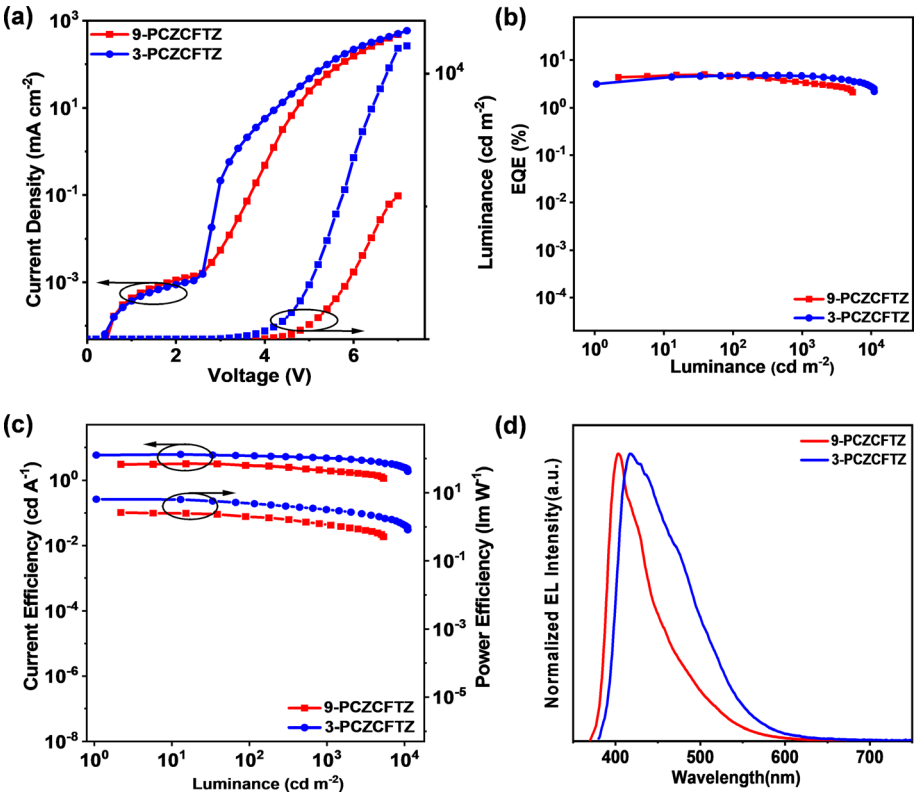

Fig. 5 Non-doped OLED performances of the two D–π–A materials. (a) Current density–voltage–luminance curves, (b) EQE–luminance curves, (c) current efficiency–luminance–power efficiency curves, and (d) EL spectra.

Table 2 Summary of the non-doped (N1, N2) and doped (D1, D2) OLED performances of the two materials

Emitter	V_{on}[a] [V]	EQE_{max}[b] [%]	CE_{max}[c] [cd A^{-1}]	PE_{max}[d] [lm W^{-1}]	L_{max}[e] [cd m^{-2}]	EL[f] [nm]	CIE (x, y)
N1	3.6	5.0	3.2	3.0	5386	404	0.160, 0.100
N2	2.8	4.8	6.1	6.5	11 044	417	0.158, 0.135
D1	5.0	14.5	2.1	1.3	1423	390	0.162, 0.045
D2	4.6	10.8	2.7	1.7	2990	398	0.159, 0.051

[a] V_{on}: turn-on voltage at 1 cd m^{-2}. [b] EQE_{max}: maximum EQE. [c] CE_{max}: maximum current efficiency. [d] PE_{max}: maximum power efficiency. [e] L_{max}: maximum luminance. [f] EL: EL peak wavelength.

ability of CBP also provides faster hole transmission channels for the two molecules. Remarkably, two-to-four-fold improvements were attained for the EQE values in both molecules, confirming that high device performance can be achieved by tuning the mobilities in doped devices to obtain excellent EQE with high color quality from the stacking mode in the single crystal, which can be regarded as a potentially useful strategy for producing highly efficient NUV OLEDs.

Conclusions

In conclusion, two blue-to-NUV D–π–A materials were designed and synthesized using an innovative route. Their non-doped OLEDs exhibit EL peaks in the range of 404–417 nm with ordinary EQE values. Notably, the electron mobilities are higher than the hole mobilities for both materials, benefiting from the excellent electron transport capacities and small torsion of TZ. In addition, the greater planarity of **9-PCZCFTZ** contributes to richer intermolecular forces, leading to more balanced carrier mobility for **9-PCZCFTZ**. However, the unbalanced carrier transport performance makes it hard to improve the efficiency. This means, that despite the impact of energy transfer, the EQE values of the two materials can be significantly improved in the doped device, particularly for **9-PCZCFTZ**, for which the EQE increased from 5.0% to 14.5% by dispersing the guest material into CBP, which has strong hole-transport ability. In summary, the present work provides a clear explanation of a novel strategy to achieve high efficiency in doped devices.

Data availability

The data supporting this article have been included as part of the ESI. Additional data are available from the corresponding author upon reasonable request.†

Author contributions

H. Zhou conducted the synthesis and basic property characterizations and wrote the manuscript. R. Wang performed the fabrication and characterization studies of the devices and review the content of this article. M. Sun contributed to editing the article. Y. Zhou, L. Zhang, J. Song and Q. Sun helped to reviewed and revised it. S.-T. Zhang supported the theoretical calculations. S. Xue, W. Yang, and S.-T. Zhang conceived the idea, and supervised this study.

Conflicts of interest

There are no conflicts to declare.

Acknowledgements

This work is supported by the National Natural Science Foundation of China (No. 51873095 and 52273183), Taishan Scholar Constructive Engineering Foundation of Shandong Province of China (No. tsqn202211164), the Natural Science Foundation of Qingdao City of China (No. 23-2-1-239-zyyd-jch). We also thank the Open Project of the State Key Laboratory of Supramolecular Structure and Materials of Jilin University (sklssm2023029).

Notes and references

1 C. W. Tang and S. A. VanSlyke, *Appl. Phys. Lett.*, 1987, **51**, 913–915.
2 J. Han, Z. Huang, J. Miao, Y. Qiu, Z. Xie and C. Yang, *Chem. Sci.*, 2022, **13**, 3402–3408.
3 X. H. Lv, L. Xu, W. Cui, Y. Yu, H. Y. Zhou, M. Cang, Q. K. Sun, Y. Y. Pan, Y. W. Xu, D. H. Hu, S. F. Xue and W. J. Yang, *ACS Appl. Mater. Interfaces*, 2021, **13**, 970–980.
4 K. T. Kamtekar, A. P. Monkman and M. R. Bryce, *Adv. Mater.*, 2010, **22**, 572–582.
5 K. E. Linton, A. L. Fisher, C. Pearson, M. A. Fox, L.-O. Pålsson, M. R. Bryce and M. C. Petty, *J. Mater. Chem.*, 2012, **22**, 11816–11825.
6 H. Qi, D. Xie, Z. Gao, S. Wang, L. Peng, Y. Liu, S. Ying, D. Ma and S. Yan, *Chem. Sci.*, 2024, **15**, 11053–11064.
7 H. Park, A. Maheshwaran, C. Moon, H. Lee, S. Reddy, V. Sree, J. Yoon, J. Kim, J. Kwon, J. Kim and S. Jin, *Adv. Mater.*, 2020, **32**, 2002120.
8 H. Lee, R. Braveenth, J. Park, C. Jeon, H. Lee and J. Kwon, *ACS Appl. Mater. Interfaces*, 2022, **14**, 36927–36935.
9 C. Chan, Y. Lee, M. Mamada, K. Goushi, Y. Tsuchiya, H. Nakanotani and C. Adachi, *Chem. Sci.*, 2022, **13**, 7821–7828.
10 G. Li, B. Li, H. Zhang, X. Guo, C. Lin, K. Chen, Z. Wang, D. Ma and B. Tang, *ACS Appl. Mater. Interfaces*, 2022, **14**, 10627–10636.
11 H.-J. Tan, J.-R. Yu, Z.-Z. Lin, G.-X. Yang, Z.-Q. Long, Y.-L. Deng, Z.-L. Zhu, X.-K. Chen, J.-X. Jian, Q.-X. Tong and C.-S. Lee, *Chem. Eng. J.*, 2024, **481**, 148567.
12 H. Tan, G. Yang, Y. Deng, C. Cao, J. Tan, Z. Zhu, W. Chen, Y. Xiong, J. Jian, C. Lee and Q. Tong, *Adv. Mater.*, 2022, **34**, 2200537.
13 W. Qin, Z. Yang, Y. Jiang, J. Lam, G. Liang, H. Kwok and B. Tang, *Chem. Mater.*, 2015, **27**, 3892–3901.
14 Y. Gao, S. Zhang, Y. Pan, L. Yao, H. Liu, Y. Guo, Q. Gu, B. Yang and Y. Ma, *Phys. Chem. Chem. Phys.*, 2016, **18**, 24176–24184.
15 X. Lv, M. Sun, L. Xu, R. Wang, H. Zhou, Y. Pan, S. Zhang, Q. Sun, S. Xue and W. Yang, *Chem. Sci.*, 2020, **11**, 5058–5065.
16 H. Uoyama, K. Goushi, K. Shizu, H. Nomura and C. Adachi, *Nature*, 2012, **492**, 234–238.
17 G. Zhao, D. Liu, P. Wang, X. Huang, H. Chen, Y. Zhang, D. Zhang, W. Jiang, Y. Sun and L. Duan, *Angew. Chem., Int. Ed.*, 2022, **61**, e202212861.
18 L. Liang, C. Qu, X. Fan, K. Ye, Y. Zhang, Z. Zhang, L. Duan and Y. Wang, *Angew. Chem., Int. Ed.*, 2024, **63**, e202316710.
19 H. Wang, J. X. Chen, Y. Z. Shi, X. Zhang, L. Zhou, X. Y. Hao, J. Yu, K. Wang and X. H. Zhang, *Adv. Mater.*, 2024, **36**, 2307725.
20 D. Zhang and L. Duan, *Nat. Photonics*, 2021, **15**, 173.
21 Y. Liu, H. Liu, Q. Bai, C. Du, A. Shang, D. Jiang, X. Tang and P. Lu, *ACS Appl. Mater. Interfaces*, 2020, **12**, 16715–16725.
22 X. Tang, Q. Bai, Q. Peng, Y. Gao, J. Li, Y. Liu, L. Yao, P. Lu, B. Yang and Y. Ma, *Chem. Mater.*, 2015, **27**, 7050–7057.
23 H. Zhang, G. Li, X. Guo, K. Zhang, B. Zhang, X. Guo, Y. Li, J. Fan, Z. Wang, D. Ma and B. Z. Tang, *Angew. Chem., Int. Ed.*, 2021, **133**, 22415.
24 D. Ahn, S. Kim, H. Lee, I. Ko, D. Karthik, J. Lee and J. Kwon, *Nat. Photonics*, 2019, **13**, 540–546.
25 D. Ahn, H. Lee, S. Kim, D. Karthik, J. Lee, H. Jeong, J. Lee and J. Kwon, *ACS Appl. Mater. Interfaces*, 2019, **11**, 14909–14916.
26 M. Hempe, A. K. Harrison, J. S. Ward, A. S. Batsanov, M. A. Fox, F. B. Dias and M. R. Bryce, *J. Org. Chem.*, 2021, **86**, 429–445.
27 R. Wang, T. Li, C. Liu, M. Xie, H. Zhou, Q. Sun, B. Yang, S. Zhang, S. Xue and W. Yang, *Adv. Funct. Mater.*, 2022, **32**, 2201143.
28 H. Zhou, T. Li, M. Xie, Y. Zhou, Q. Sun, S.-T. Zhang, Y. Zhang, W. Yang and S. Xue, *Chem. Sci.*, 2024, **15**, 8106–8111.
29 R. Wu, K. Sun, G. Shi, Y. Han, T. Gong, Y. Xu, S.-T. Zhang and B. Yang, *Adv. Funct. Mater.*, 2024, **34**, 202403501.
30 H. Wu, G. Li, J. Luo, T. Chen, Y. Ma, Z. M. Wang, A. Qin and B. Z. Tang, *Adv. Opt. Mater.*, 2021, **9**, 2101085.
31 Y. Luo, S. Li, Y. Zhao, C. Li, Z. Pang, Y. Huang, M. Yang, L. Zhou, X. Zheng, X. Pu and Z. Lu, *Adv. Mater.*, 2020, **32**, 2001248.
32 Y. Zheng, X. Zhu, Z. Ni, X. Wang, Z. Zhong, X. Feng, Z. Zhao and H. Lu, *Adv. Opt. Mater.*, 2021, **9**, 2100965.
33 X. Han, Q. Bai, L. Yao, H. Liu, Y. Gao, J. Li, L. Liu, Y. Liu, X. Li, P. Lu and B. Yang, *Adv. Funct. Mater.*, 2015, **25**, 7521–7529.
34 M. Stanitska, M. Mahmoudi, N. Pokhodylo, R. Lytvyn, D. Volyniuk, A. Tomkeviciene, R. Keruckiene, M. Obushak and J. Grazulevicius, *J. Org. Chem.*, 2022, **87**, 4040–4050.
35 T. Chiu, H. Chen, Y. Hsieh, J. Huang and M. Leung, *J. Phys. Chem. C*, 2015, **119**, 16846–16852.
36 J. Shi, Q. Ding, L. Xu, X. Lv, Z. Liu, Q. Sun, Y. Pan, S. Xue and W. Yang, *J. Mater. Chem. C*, 2018, **6**, 11063–11070.